JACS
JOURNAL OF THE AMERICAN CHEMICAL SOCIETY

Subscriber access provided by INSTITUTE OF CHEMISTRY

Article

Polymer Solar Cells: Solubility Controls Fiber Network Formation

Jacobus J. van Franeker, Gaël H. L. Heintges, Charley Schaefer, Giuseppe Portale, Weiwei Li, Martijn M. Wienk, Paul van der Schoot, and René A. J. Janssen

J. Am. Chem. Soc., **Just Accepted Manuscript** • DOI: 10.1021/jacs.5b07228 • Publication Date (Web): 26 Aug 2015

Downloaded from http://pubs.acs.org on September 1, 2015

Just Accepted

"Just Accepted" manuscripts have been peer-reviewed and accepted for publication. They are posted online prior to technical editing, formatting for publication and author proofing. The American Chemical Society provides "Just Accepted" as a free service to the research community to expedite the dissemination of scientific material as soon as possible after acceptance. "Just Accepted" manuscripts appear in full in PDF format accompanied by an HTML abstract. "Just Accepted" manuscripts have been fully peer reviewed, but should not be considered the official version of record. They are accessible to all readers and citable by the Digital Object Identifier (DOI®). "Just Accepted" is an optional service offered to authors. Therefore, the "Just Accepted" Web site may not include all articles that will be published in the journal. After a manuscript is technically edited and formatted, it will be removed from the "Just Accepted" Web site and published as an ASAP article. Note that technical editing may introduce minor changes to the manuscript text and/or graphics which could affect content, and all legal disclaimers and ethical guidelines that apply to the journal pertain. ACS cannot be held responsible for errors or consequences arising from the use of information contained in these "Just Accepted" manuscripts.

ACS Publications

Journal of the American Chemical Society is published by the American Chemical Society. 1155 Sixteenth Street N.W., Washington, DC 20036
Published by American Chemical Society. Copyright © American Chemical Society. However, no copyright claim is made to original U.S. Government works, or works produced by employees of any Commonwealth realm Crown government in the course of their duties.

Polymer Solar Cells: Solubility Controls Fiber Network Formation

Jacobus J. van Franeker,[†,‡] Gaël H. L. Heintges,[†] Charley Schaefer,[§,‡] Giuseppe Portale,[¶] Weiwei Li,[⊥] Martijn M. Wienk,[†,‖] Paul van der Schoot,[§] and René A. J. Janssen*[,†,‖]

[†] Molecular Materials and Nanosystems & Institute for Complex Molecular Systems, Eindhoven University of Technology, P.O. Box 513, 5600 MB Eindhoven, The Netherlands

[‡] Dutch Polymer Institute (DPI), P.O. Box 902, 5600 AX Eindhoven, the Netherlands

[§] Theory of Polymers and Soft Matter, Eindhoven University of Technology, P.O. Box 513, 5600 MB Eindhoven, The Netherlands

[¶] DUBBLE CRG BM26@ESRF, Netherlands Organization for Scientific Research (NWO), 71 Avenue des Martyrs, 38000 Grenoble, France.

[⊥] Beijing National Laboratory for Molecular Sciences, CAS Key Laboratory of Organic Solids, Institute of Chemistry, Chinese Academy of Sciences, Beijing 100190, P. R. China.

[‖] Dutch Institute for Fundamental Energy Research, De Zaale 20, 5612 AJ Eindhoven, The Netherlands

Abstract

The photoactive layer of polymer solar cells is commonly processed from a four-component solution, containing a semiconducting polymer and a fullerene derivative dissolved in a solvent-cosolvent mixture. The nanoscale dimensions of the polymer-fullerene morphology that is formed upon drying determines the solar cell performance, but the fundamental processes that govern the size of the phase-separated polymer and fullerene domains are poorly understood. Here we investigate morphology formation of an alternating co-polymer of diketopyrrolopyrrole and a thiophene-phenyl-thiophene oligomer (PDPPTPT) with relatively long 2-decyltetradecyl (DT) sidechains blended with [6,6]-phenyl-C_{71}-butyric acid methyl ester. During solvent evaporation the polymer crystallizes into a fibrous network. The typical width of these fibers is analyzed by quantification of transmission electron microscopic images, and is mainly determined by the solubility of the polymer in the cosolvent and the molecular weight of the polymer. A higher molecular weight corresponds to a lower solubility and film processing results in a smaller fiber width. Surprisingly, the fiber width is not related to the drying rate or the amount of cosolvent. We made solar cells with fiber widths ranging from 28 to 68 nm and find an inverse relation between fiber width and photocurrent. Finally, by mixing two cosolvents we develop a ternary solvent system to tune the fiber width. We propose a model based on nucleation-and-growth which can explain these measurements. Our results show that the width of the semicrystalline polymer fibers is not the result of a frozen dynamical state, but determined by the nucleation induced by the polymer solubility.

1. Introduction

The promise of polymer solar cells is mainly fueled by their solution-processability which allows for large-scale, roll-to-roll production of flexible solar cells.[1] The active layer is the most important layer of these solar cells, but also the most complex, as it consists of two different solid components: a semiconducting polymer as electron donor and a fullerene-derivative as an electron acceptor. For solution processing both components are dissolved in a common solvent or solvent mixture. During the evaporation of the solvents the two solid components phase separate, and form a certain morphology termed a bulk-heterojunction.[2] The importance of the exact nanoscale morphological structure has been long recognized and is studied intensively.[3]

A common strategy to obtain the highly intermixed bulk-heterojunction is to use solvent mixtures: a small amount of a cosolvent is added to the main solvent. In general, the main solvent needs to be a good solvent for the polymer and the fullerene, while the cosolvent must evaporate slower than the main solvent, and has to have a selective solubility for the fullerene.[4-6] For semicrystalline polymers these cosolvent properties cause the polymer to aggregate in a relatively dilute solution during solvent evaporation.[7,8] When the polymer aggregates, the fullerene is still dissolved and will then solidify in the regions between the crystalline aggregates. The aggregation of these semicrystalline polymers can result in the formation of polymer fiber networks.[9-12]

The ideal length scale for a polymer solar cell morphology is in the order of the exciton diffusion length, which is about 5 - 10 nm.[13] The width of the polymer fibers in the fiber network thus needs to be on the order of 10 nm or less. However, the ideal thickness of the solar cells exceeds 100 nm in order to achieve full absorption of the incident light. This difference in required length scale, combined with the small size, limits our ability to visualize and study the morphology of optimized polymer solar cells. Most commonly transmission electron microscopy (TEM) is used to characterize the morphology of polymer solar cells, but the overlapping of the fibers prevents the quantitative analysis of these morphologies and at most qualitative trends can be identified.

The current record power conversion efficiency (PCE) for a single-junction polymer solar cell of 10.8% has been achieved by optimizing the temperature-dependent aggregation behavior.[14] In that study large effects were found of both molecular weight and side chain length, which were shown to have an important impact on aggregation and performance. Both relations, that of molecular weight and morphology,[15-19] and that of side chain length and domain size[10,20] have also been identified previously. Also, very recently it was demonstrated that the solubility of the polymer in different cosolvents controls the width of the polymer fibers.[21]

In this contribution we study the effect of polymer molecular weight and processing on the typical length scales of the polymer fiber networks for a diketopyrrolopyrrole-based copolymer. By developing quantification methods we discover that many processing parameters that were thought to be important do not have a significant influence on the fiber width; most notably the polymer:fullerene ratio, the amount of cosolvent, and the solvent evaporation rate *do not* change the width of the fibers significantly. This indicates that the fiber width is not limited

by their growth after initial formation. We find that the molecular weight of the polymer and the type of cosolvent *do* have a large influence on the width of polymer fibers. We also tune the width of polymer fibers in solar cells by processing from ternary solvent blends, in which two cosolvents are used simultaneously. We propose a model based on nucleation-and-growth of individual fiber nuclei as a mechanism to explain the observed solubility-dependent fiber width. Experimentally, a convenient handle to predict trends in the typical length scale of fiber networks is the polymer solubility in the cosolvent.

2. Results

To study the processing parameters that influence morphology, a semicrystalline polymer which has been shown to give relatively wide fibers and a coarser morphology was employed, as the larger length scales are easier to study quantitatively with TEM than the small length scales usually seen in optimized materials. This alternating copolymer (DT-PDPPTPT) consists of electron-donating thiophene-phenyl-thiophene (TPT) oligomers and electron-withdrawing diketopyrrolopyrrole (DPP) groups with relatively long 2-decyltetradecyl (DT) side chains.[10] In our previous study, the DT-PDPPTPT:[70]PCBM ([6,6]-phenyl-C_{71}-butyric acid methyl ester) mixture was processed from chloroform (CF) with 1,8-diiodooctane (DIO) as cosolvent, which resulted in a relatively low PCE of 3.2%.[10] This was attributed to the large width of the polymer fibers of approximately 30 nm that were formed under these conditions. In this contribution, we used a newly synthesized batch of the same DT-PDPPTPT, which we abbreviate as P00. We found that even wider fibers could be obtained when 1,2-dichlorobenzene (*o*DCB) was used as cosolvent and thus we used the chloroform-*o*DCB solvent combination for our reference device. This device was processed on indium tin oxide (ITO) covered glass substrates, which were coated with a poly(ethylenedioxythiophene):poly(styrene sulfonate) (PEDOT:PSS) hole-collection layer. The electron collecting contact was made by thermal evaporation of a 1 nm lithium fluoride layer, followed by depositing 100 nm aluminum. The studied processing parameters are detailed in Table 1. Further experimental details are found in the Supplementary Information, Section S1.

2.1. Effects of the fullerene derivative and blend ratio

The P00 polymer was blended with three different fullerene derivatives, viz. [6,6]-phenyl-C_{61}-butyric acid methyl ester ([60]PCBM), [6,6]-phenyl-C_{71}-butyric acid methyl ester ([70]PCBM) [70]PCBM, and indene-C_{60} bisadduct (ICBA) to study the effect of the fullerene on the film formation. Figure 1 shows the TEM images of the P00:fullerene blend layers cast from chloroform:*o*DCB (94:6 v/v). The fiber network seen in TEM images is caused by polymer crystallization.[7,8,22] This can be seen in the zoomed inset in Figure 1: the crystalline fringes only appear in the polymer fibers. The distance between the fringes can be extracted from a Fourier transform and matches the expected lamellar stacking distance of ~2.2 – 2.4 nm. The crystallinity of DT-PDPPTPT fiber networks is confirmed by the grazing-incidence wide-angle X-ray scattering (GIWAXS) measurements shown in Figure 2. Both the pure polymer, and the polymer mixed with [70]PCBM show diffracted rings and arcs typical of a semicrystalline structure similarly to the ones shown by other semiconducting polymers.[3] A main reflection is observed in both the in-plane and out-of-plane direction with a stacking distance d of ~2.4 - 2.5 nm ($d = 2\pi/q_{max}$ with q_{max} ~ 2.5-2.6 nm^{-1}), in agreement with the distance extracted from the fringes in the TEM images. This reflection is assigned to the lamellar stacking. In addition, two broad peaks confirming molecular packing are observed centered at a distance of 0.48 nm (q_{max} ~ 13.0 nm^{-1}) and at 0.38 nm (q_{max} ~ 16.4 nm^{-1}). The latter one is in agreement with typical values reported for the π-π stacking distance in most of the semiconducting polymers.[3] When [70]PCBM is added, these reflections are overlapped with the [70]PCBM ring at q_{max} ~ 13.3 nm^{-1}.

The main morphological features in the TEM images are the polymer fiber networks, and it is thus expected that the typical length scales of these fiber networks are mainly determined by the polymer, and not by the properties of the used fullerene. Solar cells with varying fullerene type or polymer:fullerene ratios were made to verify this hypothesis. The solar cell performance is detailed in Table 1. The slightly lower short-circuit current density (J_{sc}) from the [60]PCBM device is expected, because of its lower absorption compared to [70]PCBM. When ICBA is used, the photocurrent is very low. This is caused by the energetic offset between the LUMO level of DT-PDPPTPT and ICBA, which is too low for exciton dissociation. Increasing the [70]PCBM content causes a decrease in photocurrent. This can be explained by optical interference effects caused by the thickness difference, and the increased spacing between the fibers, as shown in the

TEM images in Figure 1. In that case fewer excitons are able to reach a polymer:fullerene interface, where they are able to dissociate into free charges and contribute to the current.

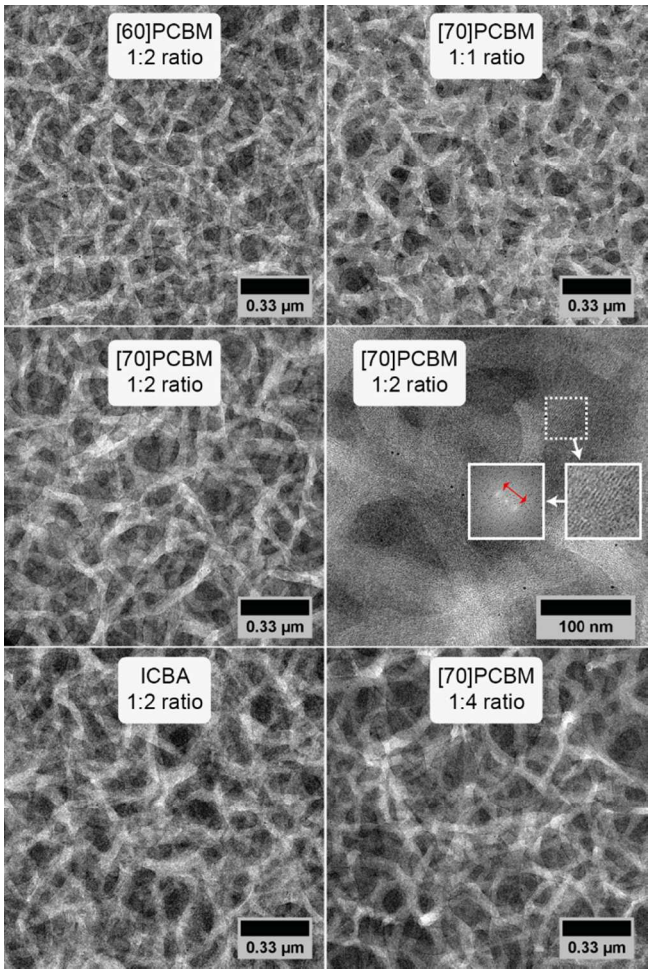

Figure 1. The effect of the used fullerene derivative on the typical size of polymer fiber networks. Films were spin coated from chloroform:*o*DCB (94:6 v/v). The left column shows that the type of fullerene only slightly influences the fiber width. The right column shows that the amount of fullerene does not significantly influence fiber width. A high-magnification TEM image of the P00:[70]PCBM film using 1:2 ratio is shown in the right column. The crystalline fringes inside the fibers can be clearly seen in the zoomed inset. A Fourier-transform of this region reveals that the lamellar stacking distance is ~2.2 – 2.4 nm.

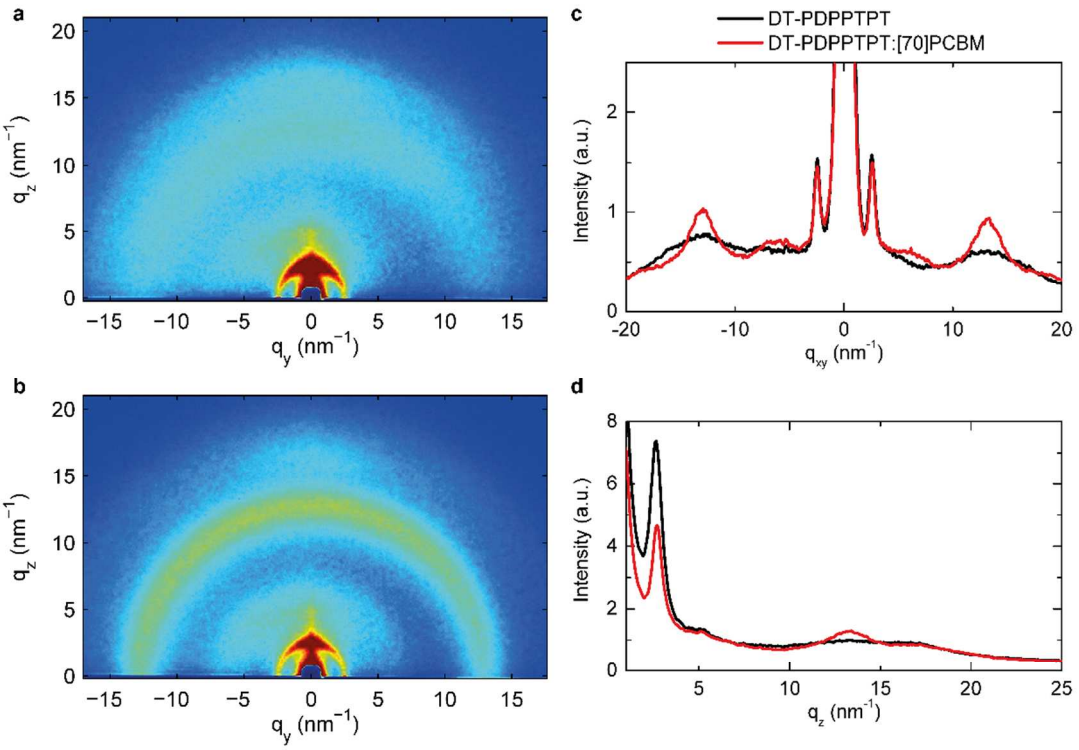

Figure 2. GIWAXS measurements on (a) a pure DT-PDDTPT film and (b) a DT-PDPPTPT:[70]PCBM film, processed from a chloroform with 5 vol. % 1,8-diiodooctane as cosolvent. In panel (c) an in-plane line cut is shown, while in panel (d) the out-of-plane line cut is shown.

The PCE of these devices is relatively low (Table 1). More interesting, however, is what we can learn about the factors that influence the morphology of these devices. The TEM images shown in Figure 1 contain information regarding the typical size of the polymer fiber networks. The device with [60]PCBM has slightly narrower fibers than the [70]PCBM or ICBA devices. The P00:[70]PCBM ratio does not seem to influence the fiber width significantly, although the inter-fiber distance obviously increases.

Drawing general conclusions based on a single TEM image of each device can be misleading. Thus, for each device at least five images were used for a quantitative analysis of the typical length scale. Contrary to high-performing solar cells in which length scales are too small for reliable quantitative analysis, these networks of large fibers allow for a relatively simple quantification. However, an unambiguous determination of length scales is not trivial. Three different quantitative methods were used to verify trends and to study different aspects of the

morphology. A Fourier-transform (FT) approach can give insight in the relative frequency with which different length scales appear. The difference between fiber width and length complicates this analysis, but in many cases a peak can be found for a typical length scale. A second approach is to use an edge-fitting algorithm. Here, we use the Canny edge-detection [23] implemented in Wolfram Mathematica 10. This algorithm detects gradients in contrast and thus detects the edges of the fibers. A intercept or segment length can be defined as the distance between two of these detected edges.[24,25] The edge-based mean segment length (EMSL) is calculated as the mean of all the segment lengths on all horizontal and vertical lines. Both these methods are sensitive to both the fiber width and the mesh size (or inter-fiber distance) of the fiber networks. To quantify the fiber width separately, as a third option we attempt to quantify the fiber width using a binarization of the TEM-images.[26,27] On these binary images, a medial axis transform or skeleton-transform (ST) is applied,[28] which gives the midlines of the polymer fibers. The pixel value of these lines is given by the distance of that point to the background, which relates to half of the fiber width. This third method is less robust and computationally more intensive than the other two methods. Because of this, it is important to verify that the trends we observe hold for all quantification methods. In our discussion we will mainly use the third method, the quantification of the fiber width, because this is the clearest morphological feature. This is legitimized by Figure S6, in which we show that there is a strong correlation between the different quantification methods. For a detailed description of these quantification methods, see Supplementary Information, Section S2.

Table 1 shows the quantification results for the TEM images shown in Figure 1. As we already concluded from the visual inspection, all quantification methods indicate that the device with [60]PCBM has slightly smaller length scales. The ICBA-device is very similar to the [70]PCBM device. Finally, increasing the amount of [70]PCBM causes the quantification using FT and EMSL to increase, because the inter-fiber distance increases. However, the ST quantification does not significantly increase, indicating that the fiber width does not change significantly. Combined, these experiments show that the influence of the fullerene type or P00:fullerene ratio on the width of the polymer fibers is limited.

Table 1. Detailed Processing Parameters, Solar Cell Performance, and Size Quantification

Polymer fraction	C [a] (mg mL^{-1})	Fullerene	Ratio (w/w)	Cosolvent	Cosolvent (vol. %)	Spin speed (rpm)	d [b] (nm)	J_{sc} [c] (mA cm^{-2})	V_{oc} [c] (V)	FF [c] (%)	PCE (%)	FT (nm)	EMSL (nm)	ST [e] (nm)
P00	5	[60]PCBM	1:2	oDCB	6	2000	124	4.83	0.80	70	2.7	261	68	21
P00	5	[70]PCBM	1:2	oDCB	6	2000	123	5.68	0.80	67	3.0	312	76	24
P00	5	ICBA	1:2	oDCB	6	2000	132	0.34	0.96	48	0.2	331	75	24
P00	5	[70]PCBM	1:1	oDCB	6	2000	100	6.15	0.80	72	3.5	253	71	22
P00	5	[70]PCBM	1:2	oDCB	6	2000	128	5.29	0.79	70	2.9	337	76	25
P00	5	[70]PCBM	1:4	oDCB	6	2000	190	4.47	0.79	64	2.3	556	78	24
P00	5	[70]PCBM	1:2	oDCB	6	2000	114	5.84	0.79	71	3.3	270	69	22
P30	5	[70]PCBM	1:2	oDCB	6	2000	99	4.12	0.83	69	2.4	384	94	28
P40	5	[70]PCBM	1:2	oDCB	6	2000	87	4.34	0.82	68	2.4	341	96	28
P50	5	[70]PCBM	1:2	oDCB	6	2000	93	5.04	0.82	68	2.9	328	83	27
P65	5	[70]PCBM	1:2	oDCB	6	2000	120	5.97	0.81	67	3.2	313	71	22
P90	5	[70]PCBM	1:2	oDCB	6	2000	161	8.28	0.78	69	4.4	242	61	18
P90	5	[70]PCBM	1:2	oDCB	6	3000	120	8.46	0.79	68	4.6	242	61	18
P00	3	[70]PCBM	1:2	oDCB	3.6	500	110	5.88	0.81	70	3.3	267	68	22
P00	4	[70]PCBM	1:2	oDCB	4.8	1000	116	5.58	0.81	71	3.2	280	74	24
P00	5	[70]PCBM	1:2	oDCB	6.0	2000	122	5.59	0.80	70	3.1	293	67	22
P00	6.5	[70]PCBM	1:2	oDCB	7.8	5000	112	5.83	0.81	70	3.3	284	76	24
P00	5	[70]PCBM	1:2	oDCB	5	2000	130	5.02	0.78	64	2.5	380	81	26
P00	5	[70]PCBM	1:2	CN	5	2000	132	5.42	0.79	66	2.8	280	66	21
P00	5	[70]PCBM	1:2	DIO	5	2000	130	8.62	0.78	65	4.4	-	54	15
P00	5	[70]PCBM	1:2	DPE	5	2000	136	8.96	0.77	63	4.4	-	53	14
P90	5	[70]PCBM	1:2	DIO	5	3000	177	10.2	0.77	62	4.9	-	54	14
P00	5	[70]PCBM	1:2	oDCB	5	2000	112	4.92	0.79	65	2.5	333	80	26
P00	5	[70]PCBM	1:2	oDCB:DIO	4.5:0.5	2000	108	5.2[d]	0.79	66	2.7	250	68	20
P00	5	[70]PCBM	1:2	oDCB:DIO	4:1	2000	115	7.23	0.78	65	3.7	229	63	18
P00	5	[70]PCBM	1:2	oDCB:DIO	3.1:1.9	2000	126	8.47	0.77	64	4.2	221	55	15
P00	5	[70]PCBM	1:2	DIO	5	2000	128	8.86	0.77	64	4.4	-	56	15
P00[f]	5	[70]PCBM	1:2	oDCB	5 or 6	2000	122 ± 8	5.39 ±0.37	0.79 ±0.01	67.8 ±2.9	2.9 ±0.3	321 ± 38	75 ± 6	24 ± 2

[a] Concentration of polymer in spin casting solution. [b] Film thickness. [c] J_{sc} is obtained by integrating the EQE-measurement with the AM1.5G spectrum, V_{oc} is open-circuit voltage, FF is fill factor. [d] No EQE, *J-V*-value corrected using other cells of the same day. [e] The value determined with the ST-method corresponds to half of the fiber width. [f] Average of the six devices processed using these parameters.

2.2. Effect of the molecular weight

It has been shown before that the molecular weight of the polymer influences the solar cell performance.[15-19, 29 , 30] This has been attributed to morphological changes[15-19] or carrier mobilities.[16,19,29,30] However, there is no well-established trend between morphological length scale and molecular weight. This originates from two root causes: first, optimized solar cells often have morphological length scales too small to really quantify. Second, batch-to-batch variations other than molecular weight limit our ability to draw conclusions from molecular weight differences in different batches. Here, we used a single batch (P00, peak molecular weight M_p = 111.0 kDa) of DT-PDPPTPT. Different molecular weight fractions were extracted from this batch based on their solubility in chlorobenzene at increasing temperatures. The lowest molecular weight fraction was extracted at 30°C (P30, M_p = 88.5 kDa). Subsequent extractions were done at 40 °C (P40, M_p = 91.8 kDa), 50 °C (P50), 65 °C (P65, M_p = 114.6 kDa) and 90 °C (P90, M_p = 128.7 kDa). The trend of increasing molecular weight for extractions at higher temperature is evident. Size exclusion chromatography (SEC) traces, measured at 140 °C in oDCB, are shown in Figure 3a (details in Supplementary Information, Section S3).

Even though the differences in molecular weight are relatively limited compared to some literature examples, the effect on solar cell efficiency is striking. The current density-voltage (*J-V*) measurements (Figure 3b) and the external quantum efficiency (EQE) measurements (Figure 3c) clearly show a dramatic increase in photocurrent for increasing molecular weight. The results are also tabulated in Table 1, as well as the quantification of TEM images. Representative examples of these TEM images are shown in Figure 3d. The decreasing length scale for increased molecular weight correlates well with the increasing photovoltaic performance. The decreased domain size increases the number of excitons that can reach the polymer:fullerene interface, and thus increases the photocurrent. Also note that the differences in the typical size of these fiber networks are much larger than the small changes observed when changing the fullerene or mixing ratio (cf. Section 2.1). The effect of polymer molecular weight on fiber width is thus significantly more important than the effect of the fullerene derivative.

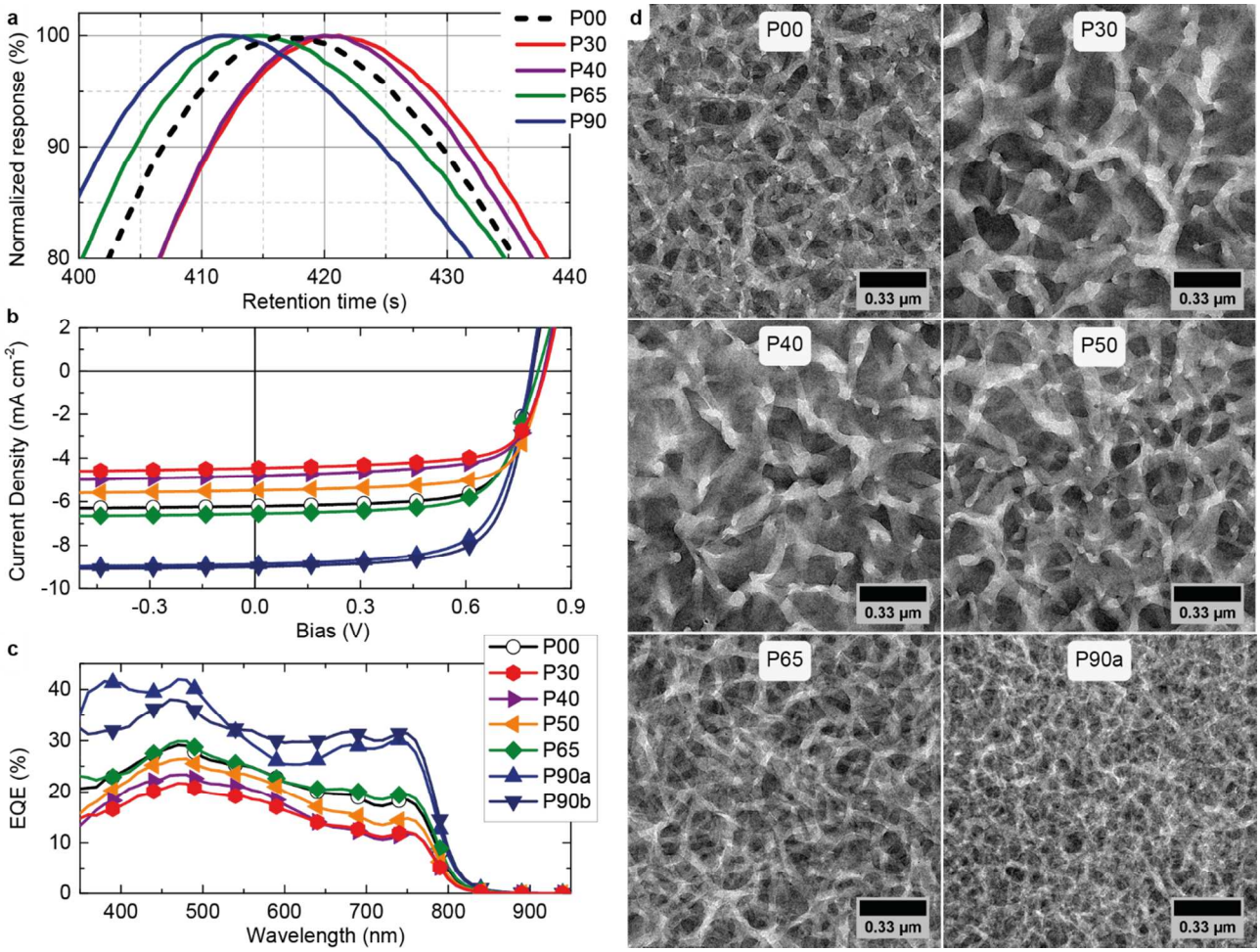

Figure 3. The effect of the polymer molecular weight on the typical size of polymer fiber networks. In panel (a) SEC traces are shown for the different polymer fractions. These fractions are used to make solar cells as detailed in Table 1. The *J-V* plots in panel (b) and the EQE in panel (c) both show a clear increase of photocurrent for increasing molecular weight. The TEM images in panel (d) show that this increased photocurrent is caused by a drastic decrease of the typical size of these fiber networks. All films are spin coated at 2000 rpm, except P90b, which is coated at 3000 rpm to obtain a thickness similar to the devices from the other polymer fractions.

2.3. Effect of the drying rate

In a previous contribution[31] we have shown that polymer:fullerene blends can form droplet-like morphologies when processed from a single solvent due to liquid-liquid phase separation.[32,33] Typical length scales in these droplet-like morphologies depend on the normalized drying rate,

which is defined as the rate of thickness change due to solvent evaporation, divided by the final thickness.[27]

For the morphologies with fiber networks, processed from a solvent/cosolvent mixture, we hypothesized that a slower normalized drying rate would lead to larger typical length scales as well. However, due to the solvent/cosolvent mixture an unambiguous definition of normalized drying rate is impossible because the two solvents evaporate at different rates. Still, we are able to change the normalized drying rate by simultaneously increasing the solution concentration and the spin speed. If the cosolvent/solid ratio is kept constant the evolution of thickness with time (Figure 4a) can be normalized with respect to time (Figure 4b), such that all drying curves overlap. This means only the normalized drying rate has changed. For more information on the measurement of these drying curves, see ref. 27 or Supplementary Information, Section S1.

The detailed processing settings are shown in Table 1. Film thickness and the solar cell performance parameters are all very similar. This is in accordance with their similarity in morphology as seen in the TEM images (Figure 4c, quantification in Table 1). These results were contrasting with our initial hypothesis, as we expected that the factor three increase in drying rate would lead to a smaller typical length scale. To study this in more detail, in Supporting Information, Section S4.1, we show results on a different batch of the same polymer, in which a relatively small dependence of typical length scale on the normalized drying rate was found. However, even for that batch the differences in fiber width were almost negligible compared to the differences caused by molecular weight in Section 2.2. Also, an optimized polymer with shorter 2-hecyldecyl sidechains (HD-PDPPTPT, Supplementary Information, Section S4.2) did not show any dependence of the PCE on the normalized drying rate, as all devices had a PCEs between 7.2% and 7.4%. We thus conclude that the influence of normalized drying rate on the typical size of fiber networks is at most limited.

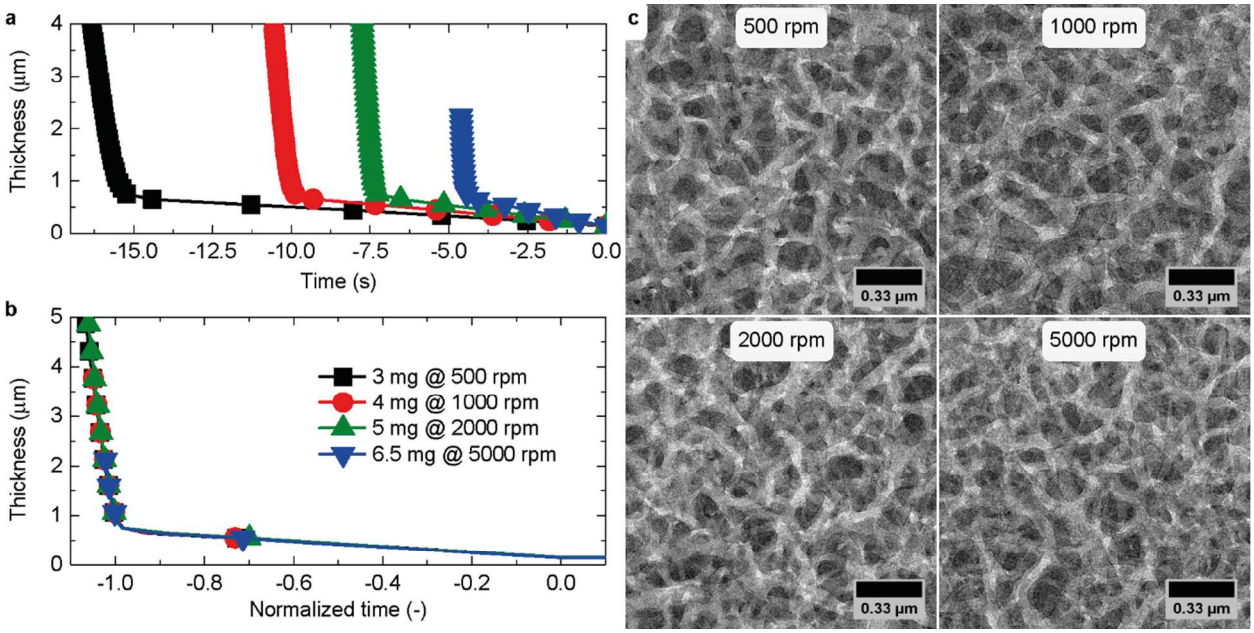

Figure 4. Four solar cells with a similar thickness are dried at different rates by increasing the solid and cosolvent concentration and simultaneously increasing the spin speed. In (a) the drying curves determined by in-situ laser interferometry are shown, where the thickness is shown as a function of the time (see Supplementary Figure S8 for details). Two regimes are visible; first the steep section in which mostly chloroform evaporates, and then the remaining oDCB evaporates much more slowly. As shown in panel (b), these curves can be normalized with respect to time (see Supplementary Figure S8 for details), showing that the thickness evolution is exactly similar albeit at different drying rates. The legend indicates the polymer concentrations and detailed processing parameters are shown in Table 1. Panel (c) shows the TEM images, which reveal that the resulting typical size of the fiber networks is not significantly influenced by the drying rate.

2.4. Effect of cosolvent type

The solar cells shown up until here are all processed from a chloroform-*o*DCB solvent mixture because the large width of resultant fibers is relatively easy to quantify. However, better solar cell performance can be reached by processing with other cosolvents. In Table 1 we show that the PCE increases from 2.5% with *o*DCB (due to the higher-than-average thickness a lower-than-average performance), via 2.8% using 1-chloronaphthalene (CN), to 4.4% using either 1,8-diiodooctane (DIO) or diphenyl ether (DPE) as cosolvent (5 vol. %). The increased efficiency is caused by the changes in typical length scale of the fiber networks (Figure 5). The (half) fiber

width, as extracted from the ST quantification, decreases from 52 to 28 nm. This leads to a higher photocurrent due to more efficient exciton splitting. The differences in fiber width caused by the nature of the cosolvent are comparable to those made using the molecular weight fractions in Section 2.2. The effect of cosolvent type is evidently much larger than any effects caused by the fullerene type or by the drying rate.

One can hypothesize that the decreasing fiber width originates from the cosolvent evaporation rate. The boiling point (b.p.) increases for the series oDCB (b.p. 180 °C) – CN (b.p. 263 °C) – DIO (b.p. 333 °C), but DPE does not adhere to this trend with a b.p. of 258 °C. For all cosolvents the evaporation rate is much slower than chloroform, which causes the amount of cosolvent to evaporate during chloroform evaporation to be small. Thus, provided that concentration of cosolvent in the initial spin casting mixture solution is constant, the quench of the polymer from solvent into cosolvent happens at similar polymer concentrations for all cosolvents. Thus, we do not expect the differences in fiber width to be caused by differences in cosolvent evaporation rate.

Another explanation relates to the solubility of the polymer in the cosolvent. This was also suggested very recently by Cao *et al.*[21] We noted that the solubility of P00 decreases in the order of decreasing fiber width for these four cosolvents. In fact, the solubility of P00 in *o*DCB is high enough to process P00:[70]PCBM solar cells from pure *o*DCB (Supplementary Information, Section S4.6). Simple solubility tests (Supplementary Information, Section S5) reveal that P00 dissolves in *o*DCB and in CN at room temperature. Only a very small fraction of P00 is soluble in DIO, as the solution turns only very light green. In DPE almost no coloration is observed. At 90 °C (solution preparation temperature) the polymer does partially dissolve or disperse in both DIO and DPE as the color changes to green. However, there are still many undissolved particles in these solutions. We thus conclude that the large differences in fiber width and PCE observed when varying the nature of the co-solvent are caused by differences in polymer solubility in the cosolvent.

To some extent the effects of molecular weight and nature of the cosolvent are additive; the smallest fibers and highest PCE (4.9%) were obtained using the high molecular weight fraction P90 of DT-PDPPTPT and 1,8-diiodooctane (DIO) as cosolvent.

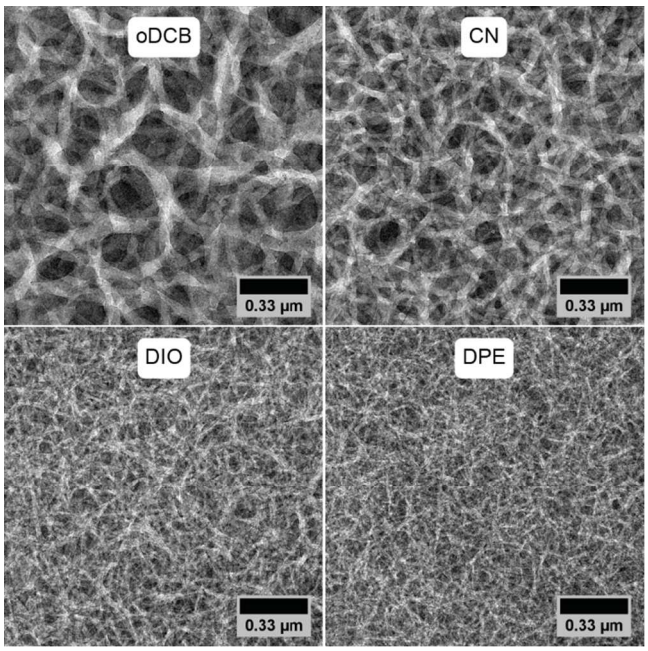

Figure 5. TEM images of P00:[70]PCBM solar cells processed from chloroform with different cosolvents (5 vol. %), as indicated in the labels.

2.5. Ternary solvent mixtures

An interesting application of the large dependence of fiber width on the nature of the cosolvent is the ability to tune the fiber width by mixing two cosolvents, thus forming a ternary solvent mixture. It has been shown before that this strategy can improve solar cell device performance.[9] We prepared P00:[70]PCBM solutions in chloroform, with a total of 5 vol. % cosolvent. Similar to the results shown in Section 2.4, the PCE increases from 2.5% when using 5% *o*DCB to 4.4% using 5% DIO due to an increased photocurrent. The cosolvent was now chosen to be a mixture of *o*DCB:DIO (v/v) as specified in Table 1. Both the TEM images in Figure 6 and the photocurrent show that morphologies in between those for the pure cosolvents can be obtained. A 4.5:0.5 ratio of *o*DCB:DIO increases the PCE to 2.7% and a 4:1 ratio to 3.7%. This shows that a small concentration of DIO in the ternary blend already has a large effect. We additionally verified this ternary-blend effect for a different batch of DT-PDPPTPT, as shown in Supplementary Information, Section S4.3.

The TEM quantification verifies that these small additions of DIO to a ternary solvent blend can already decrease the fiber width in these fiber networks. As for the cosolvent-type

effect, the smaller length scales originate in the decreased solubility of P00 due to the increased amount of DIO in the cosolvent mixture.

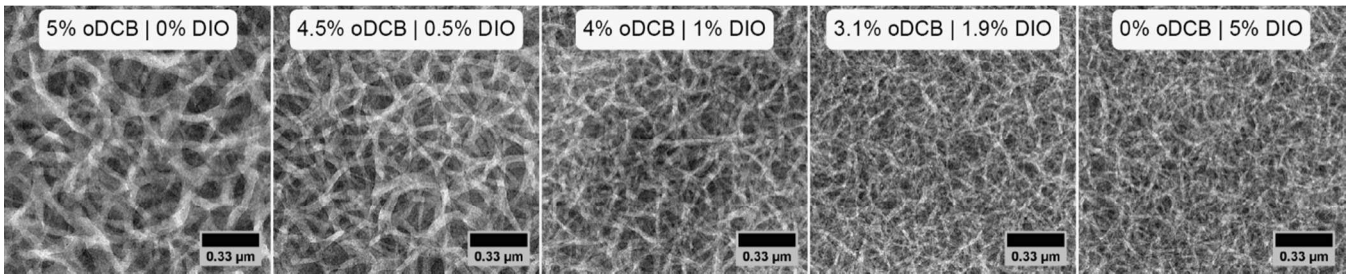

Figure 6. The typical size of the fiber networks can be tuned with ternary solvent blends. In this case a chloroform:*o*DCB:DIO mixture is used. The volume fraction of chloroform is always 95%. The volume fractions of both cosolvents are shown in the labels.

2.6. Factors with limited influence

Thermal annealing is often used to alter the morphology of organic solar cells after the wet-processing steps. For blends of poly(3-hexylthiophene) (P3HT) with [60]PCBM thermal annealing increases roughness[34] due to an increase of crystallite size.[35] In the case of P3HT this annealing step is often beneficial and even required for high photovoltaic performance. For DPP-based polymers, annealing is often not required or even detrimental for device performance. Nevertheless, we investigated the effect of thermal annealing on the typical size of polymer fibers. In the case of P00 the thermal annealing decreases the PCE due to a decrease in photocurrent (Supplementary Information, Section S4.4). However, TEM images clearly reveal that this decreased photocurrent is not caused by a change of fiber width. At present we have no consistent explanation for the decreased photocurrent after annealing. More importantly, however, thermal annealing does not significantly increase the typical size of the polymer fiber networks in these films.

In the discussions above we always used a very similar amount of cosolvent in the casting solution. We expected that the amount of cosolvent would have a large influence on the typical size of the polymer fiber networks. We thus made solar cells using different cosolvent concentrations, combined with real-time measurements of the drying process. Surprisingly, the effect of the amount of cosolvent on both photovoltaic efficiency and fiber width is very limited.

Due to the amount of data, for further discussion we refer to the Supplementary Information, Section S4.5 and S4.6.

2.7. Fiber width controls photocurrent

Due to a limited exciton diffusion length in blends of organic semiconductors,[13] there is a large dependency of the photocurrent on the morphology of organic solar cells. If length scales are too large for all excitons to reach a donor-acceptor interface, the photocurrent will increase for decreasing length scale.[10,36] Alternatively, this dependency can be thought of as a method to verify our quantification method. To check this dependency we plot the photocurrent as a function of the half fiber width (as extracted from the TEM-images using the ST method) in Figure 7. The filled symbols are the solar cells discussed in this contribution, the open symbols are additional experiments discussed in the Supporting Information. The filled symbols follow the trend of increasing photocurrent with decreasing typical length scale, as well as most open symbols. There are a few exceptions, most notably one failed device (purple triangle), the green triangles (thermal annealing decreases photocurrent, but does not influence typical length scale) and the pink pentagons (*o*DCB:DIO ratio for a different polymer batch, in which the whole series shows relatively low performance). However, the general trend is very clear, which verifies our quantification methods.

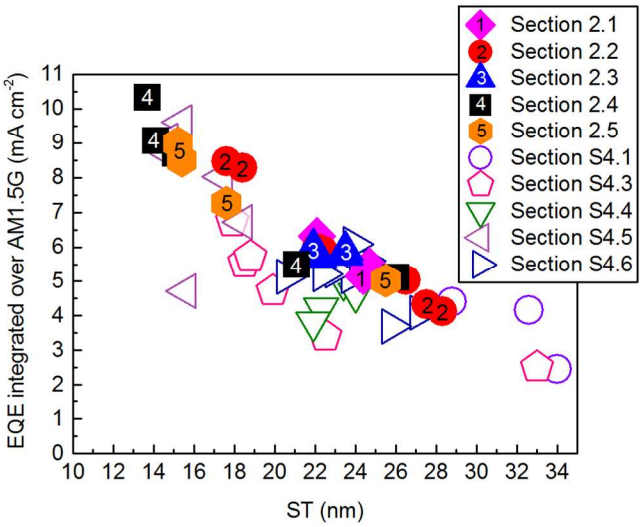

Figure 7. Dependency of photocurrent (EQE integrated over AM1.5G spectrum) on the half fiber width as extracted using the ST method. The numbers in the solid symbols refer to the

section in this article in which these devices are described. The open symbols are described in the indicated sections of the Supplementary Information.

2.8. Nucleation-and-growth of fiber networks

The results in Section 2.4 and 2.5 show that the solubility of the polymer has a large influence on the typical size of the fiber networks. To study how solvent quality could affect the formation of fiber networks, we investigate a nucleation-and-growth mechanism, in which alignment of free polymers gives rise to nucleation of fibers, which may subsequently grow into fiber networks. A schematic of this mechanism is given in Figure 8a, where we suggest that the polymer chain is oriented along the length of the fibers, as recently shown by Kim *et al.*[37] for a DPP-based polymer. In Figure 8a, we suggest that as long as there are free polymers available, both nucleus formation and growth by association of excess free polymers with aggregates may take place. Also, further growth could take place by ripening and coalescence of fibers.[38]

As an attempt to understand this nucleation-and-growth mechanism in more detail, we set up a model in the Supporting Information (Section S6). This model relies on homogeneous nucleation via classical nucleation theory[39] of cylindrical aggregates that represent fibers, and on the growth (in radial and longitudinal directions) of these aggregates via a diffusive process.[40] The growth rate depends on the difference between the free-polymer concentration and the equilibrium saturation concentration of free polymers. Nucleation and growth take place simultaneously until the excess free polymers have depleted, so that a "typical" distribution of aggregate sizes is obtained. This typical length scale of the dry-layer fiber networks can either be close to the initial nucleus size or can be mainly a result from growth. Whether the width of the fibers in the fiber networks in dry-layer morphologies is close to the initial nucleus size or is much bigger than that will depend on the growth rate compared to the nucleation rate.

To show that the observed dependencies of fiber width on solubility are compatible with a nucleation-and-growth mechanism, we fit our model to the observed fiber width of the ternary blend series (Section 2.5) for the two limiting cases of fast nucleation (Section 2.8.1) and of fast growth (Section 2.8.2). In the former case, the final length scale is related to the size of the initial nuclei as the nuclei do not have time to grow before the fast nucleation causes depletion of free polymers. In the latter case, rapid growth causes the depletion of free polymers. Then, the distribution of aggregate sizes relates to the number of nuclei formed.

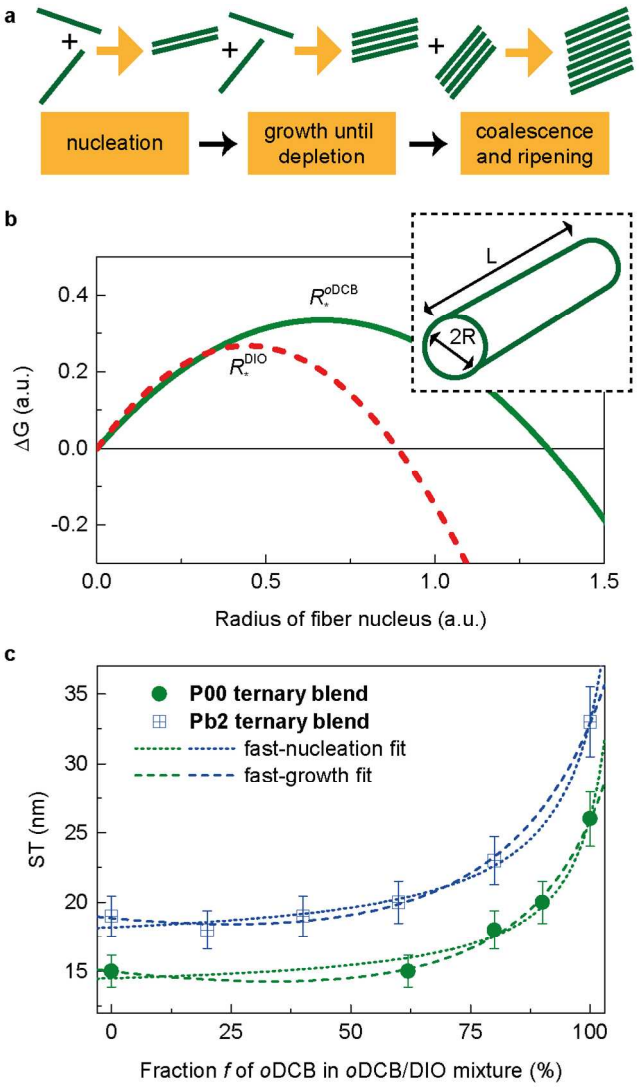

Figure 8. In panel (a) we show the mechanisms which influence the fiber width, of which we argue that nucleation and growth are dominant (Section 3), and both occur simultaneously until depletion of free polymers. Panel (b) shows a schematic of the Gibbs free energy for the formation of crystal nuclei in two solvents (see Section 2.8.1), as a function of fiber radius (Equation 1), both in arbitrary units. The inset shows the assumed geometry. Nuclei are stable when their radius is larger than the critical radius R_*. In panel (c) we fit R_{final} to the ST-based quantification of the half fiber width for the two different polymer batches processed from ternary solvent blends (symbols). The offset in fiber width between these two batches originates in the molecular weight difference, as discussed in Section 2.8.3. The error bars are calculated as

a 7.6% of the quantified size, corresponding to the standard deviation as shown in the bottom row of Table 1.

2.8.1. Fast-nucleation limit: a minimum size of stable nuclei

We assume that the fibers are cylindrical aggregates with radius *R* and length *L* (inset Figure 8b). Classical nucleation theory predicts that too small aggregates will redissolve due to an activation barrier caused by the increased surface energy. Thus, the minimum nucleus radius is determined by an activation barrier, as given by the Gibbs free energy:

$$\Delta G = L\pi R^2 \rho_S \Delta\mu + 2\pi R^2 \gamma_t + 2L\pi R\gamma \qquad (1)$$

Here, ρ_S is the number of polymers per volume. Then, $\rho_S\Delta\mu < 0$ is the chemical potential of aggregation per fiber volume, γ_t is the surface tension at the end points of the fiber, and γ is the surface tension at the sides of the fiber. A schematic plot of the Gibbs free energy (as a function of the fiber radius) is shown in Figure 8b. In the Supporting Information, Section S6.1, we show that the critical radius can be expressed as $R_* = -2\gamma/\rho_S\Delta\mu$. We now hypothesize that this minimum size of a stable nucleus is linearly related to the observed length scales as quantified by the ST method for the series with ternary solvent blends (Section 2.5). Since the interfacial energy and chemical potential depend on solvent quality, the critical radius should depend on the composition of the cosolvent mixture. To quantify how these parameters depend on solvent quality, we propose to write the surface tension and the chemical potential as a linear combination of their values in the pure cosolvents: $\gamma = f\gamma_{o\mathrm{DCB}} + (1-f)\gamma_{\mathrm{DIO}}$ and $\Delta\mu = f\Delta\mu_{o\mathrm{DCB}} + (1-f)\Delta\mu_{\mathrm{DIO}}$, where f is the fraction of *o*DCB in the *o*DCB/DIO cosolvent mixture. We can then express the critical nucleus radius as:

$$R_{final}(f) \propto R_*(f) = \frac{f + \gamma_{\mathrm{ratio}}(1-f)}{f + \Delta\mu_{\mathrm{ratio}}(1-f)} \times R_*^{o\mathrm{DCB}} \qquad (2)$$

Here, R_*^{oDCB} is the critical nucleus radius in *o*DCB, and the relative increase in surface tension and chemical potential are $\gamma_{\mathrm{ratio}} = \gamma_{\mathrm{DIO}}/\gamma_{o\mathrm{DCB}}$ and $\Delta\mu_{\mathrm{ratio}} = \Delta\mu_{\mathrm{DIO}}/\Delta\mu_{o\mathrm{DCB}}$, respectively. We then fit $R_*(f)$ to the experimental length scale as a function of *f*.

These fast-nucleation limit fits are shown in Figure 8c with dotted lines, and the values of the fit parameters are given in the Supplementary Information. We find a larger surface tension of fibers in DIO than in *o*DCB ($\gamma_{\mathrm{ratio}} = 6 \pm 3$), and larger driving force for crystallization ($\Delta\mu_{\mathrm{ratio}} = 11 \pm 5$). Also, for both data series the latter ratio is larger, thus in the poorer solvent (DIO) the increased surface tension is dominated by the larger driving force for crystallization, leading to smaller fiber nuclei. We return to the values of these fit parameters in the discussion.

2.8.2. Fast-growth limit: the number of nuclei

In the previous section we assumed that the nuclei do not have time to grow after nucleation. This assumption is only valid if the depletion of free polymers is caused by very fast nucleation. The other limiting case is the fast-growth limit, wherein the growth of aggregates is much faster than the nucleation of new aggregates. In this limit, aggregates formed will grow so fast that there is depletion of free polymers before additional nuclei can form. This can be interpreted as if just after quenching a certain number of nuclei is formed that subsequently grow, and hence that this initial number of nuclei determines the final aggregate size. As discussed in detail in the Supplementary Information, also in this limit we can find a relation of the final fiber radius as a function the fraction *f* of *o*DCB in the *o*DCB/DIO mixture:

$$\ln\frac{R_{final}(f)}{R_0} = \frac{(f+\gamma_{\mathrm{ratio}}(1-f))^3}{(f+\Delta\mu_{\mathrm{ratio}}(1-f))^2} \times \ln\frac{R_{final}^{o\mathrm{DCB}}}{R_0} \qquad (3)$$

where we set the microscopic length scale $R_0 = 1$ nm, as this factor has a limited influence on the fitted values. In Figure 8c we show the fits for the fast-growth limit described by Equation 3 with dashed lines. Also for these fits the same conclusion holds: both surface tension ($\gamma_{\mathrm{ratio}} = 1.8 \pm 0.1$) and chemical potential ($\Delta\mu_{\mathrm{ratio}} = 2.7 \pm 0.1$) are larger in the poorer solvent, but due to a larger increase of chemical potential the decreased solvent quality gives rise to a lower activation barrier. The change in Gibbs free energy is schematically shown in Figure 8b. Due to the lower activation barrier, more nuclei are formed. The increased amount of nuclei causes a smaller fiber width after all nuclei have grown until depletion of free polymers.

2.8.3. Molecular weight dependence of fiber width

The fits in Section 2.8.1 and 2.8.2 were performed for the dependence of fiber width on cosolvent quality, but a nucleation-and-growth model can also be used to explain the relation of fiber width to the molecular weight. In Section 2.2 we show that the fiber width decreases with increasing molecular weight. The solubility decreases with increasing molecular weight, which increases the thermodynamic driving force for crystallization, i.e. it makes more negative $\Delta\mu$. In the fast-nucleation limit this naturally leads to smaller fibers because the critical radius decreases as $R_* = -2\gamma/\rho_S\Delta\mu$. For the fast-growth limit, the larger $\Delta\mu$ lowers the crystallization barrier which increases the amount of nuclei formed, thus decreases the fiber width.

3. Discussion

The results presented in this paper are schematically summarized in Figure 9. It is evident that we found only two parameters which have a large influence on fiber width: the molecular weight of the polymer and the cosolvent constitution, which can be tuned by changing the cosolvent or by mixing two different cosolvents. All other investigated processing parameters have a limited to negligible influence on the fiber width. Most notable are the small influence of drying rate and amount of cosolvent.

As hypothesized in Section 2.4, the effect of the nature of the cosolvent might relate to two different properties of the cosolvent: either a decreased evaporation rate or a decreased polymer solubility might be responsible for a decreased fiber width. If we try to find a governing factor that determines the fiber width in all studied cases, only the second hypothesis is compatible with the remarkable decrease of fiber width due to increased molecular weight, as found in Section 2.2.

We thus reach the same conclusion as J. Shin *et al.*[20] and W. Li *et al.*[10] that fiber width is mainly determined by polymer solubility. This contribution specifies that the polymer solubility in the cosolvent is the crucial parameter in the determination of the width of the polymer fibers, which confirms the recent conclusion of Cao *et al.*[21]

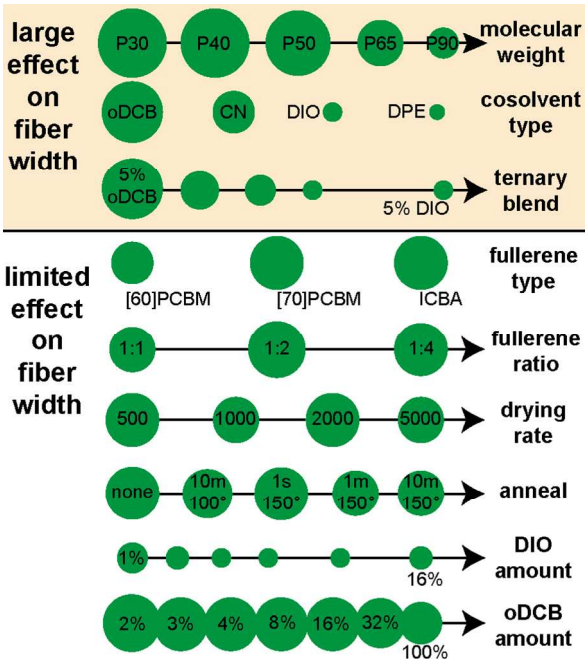

Figure 9. Graphical illustration of the changes in fiber width. The sizes of the circles are an exaggerated indication of the fiber width, as the circle radius scales as (ST-10), in which ST is the half fiber width as determined by the ST method (Table 1 and Table S2).

After this experimental observation that the fiber width is mainly determined by the solubility of the polymer in the cosolvent, we set out to understand this behavior. This ultimately led to our nucleation-and-growth model as described in Section 2.8. Before arriving at this model, we had three other hypotheses. First, we thought that the polymer solubility would influence the polymer concentration at the onset of fiber formation, which in turn would determine fiber width. Second, we thought ripening (growth after depletion of free polymer) might be influenced by polymer solubility. Third, as recently suggested by Cao *et al.*,[21] the polymer solubility might influence the amount of aggregates in the initial casting solution. All these hypotheses are realistic and might occur in other polymer systems, but they conflict at some point with our experimental observations. To clarify this, we discuss each of these hypotheses below.

In the first hypothesis, the fibers might start to form at a lower polymer concentration if the polymer solubility in the cosolvent is lower. If aggregation would indeed occur at a lower polymer concentration, this would easily explain differences in fiber width. However, the

experiments with different amounts of cosolvent described in the Supporting Information, Sections S4.5 and S4.6, show that the polymer concentration at the onset of aggregation does not influence the fiber width significantly. Furthermore, for the different cosolvents which do produce large differences in the fiber width (Section 2.4), the polymer concentration at the start of fiber formation is similar, because the aggregation onset occurs at the moment the chloroform has evaporated (which does not depend on the solubility of the polymer in the cosolvent). Thus, the concentration at which the fibers form does not determine the typical size of the polymer fiber networks.

Secondly, growth after the depletion of free polymers (the last mechanism in Figure 8a) can be influenced by the solubility of the polymer, as is shown by simulations of Groot.[38] Groot shows that for a high surface energy (low solubility) the length of the fiber network connections is limited, because after all free polymers are depleted, the fibers can only grow by coalescence. For lower surface energy (higher solubility), fibers can also grow because polymer fragments can redissolve after their initial aggregation ("ripening"). This second growth mechanism in better solvents might explain our observed solubility-dependent fiber width. However, if this were the case, a slower drying rate in these solvents would lead to thicker fibers. Our experiments in Section 2.3 show that this is not the case, as all drying rates result in similar fiber width. Also, the devices processed with an increased cosolvent concentration in Section S4.5 and S4.6 have had an increased ripening time, but also in those experiments no significant differences in fiber width are seen. Therefore, we argue that ripening is of minor importance, and growth only takes place until all free polymers are depleted from the solution.

Thirdly, a mechanism was recently suggested by Cao *et al.*[21] which is based on the presence of aggregates in the casting solution. The aggregates in the casting solution might function as "seed-crystallite nuclei" for the formation of polymer fibers. This is inspired on the paper by Schmidt *et al.*[41] in which it was shown that a cosolvent can induce aggregate formation in the casting solution. Cao *et al.*[21] propose that the type of cosolvent determines the amount of seeds in the casting solution; a solvent with a low polymer solubility would then induce more seeds, resulting in narrower fibers. In their case, for a different polymer than studied here, increasing the amount of cosolvent decreases the fiber width until a certain plateau is reached. They argue this is caused by the saturation of seed concentration in the casting solution. In our experiments, we did not find this influence of the amount of cosolvent on the fiber width. We

agree with Cao *et al.*[21] that the number of seeds or nuclei is very likely to influence the final fiber width as this is essentially the outcome of the "fast-growth" limit of our model in Section 2.8.2. The main difference with the proposed mechanism of Cao *et al.*[21] is that our model is based on homogeneous nucleation, and thus does not require the presence of aggregates in the casting solution. Also, we propose a numerical model which can be used in curve fitting. It is likely that a combination of these two idealized mechanisms occurs in reality; aggregates present in the casting solution act as seeds, but extra nuclei can be formed by homogeneous nucleation at the transition from main solvent to cosolvent.

The theoretical treatment in Section 2.8 shows that the solubility-dependent behavior of polymer fiber width can be explained by a model based on homogeneous nucleation and growth until depletion of free polymers. We do not have sufficient data to conclude whether the fiber width in these experiments is indeed related to the initial nucleus size (fast-nucleation limit) or to the amount of initial nuclei (fast-growth limit) but we can discuss whether the fitted values are sensible. The interfacial tension between the polymer and a cosolvent is proportional to the net cohesive (free) energy in the cosolvent, which in turn depends logarithmically on the solubility of the polymer in the cosolvent.[42] The fitted values in Section 2.8.1 and 2.8.2 for γ_{ratio} of 6 (respectively 1.8) would imply a net cohesive energy of that is a factor 6 (respectively 1.8) larger in DIO than in *o*DCB. This in turn implies that the polymer solubility in DIO is the 6^{th} (respectively 1.8^{th}) power of that in *o*DCB because the solubility depends exponentially on the cohesive energy.[42] Assuming a solubility of 10 mg mL^{-1} in *o*DCB (Supplementary Information Section S4.6) this leads to an implied solubility in DIO of 10^{-9} mg mL^{-1} (respectively 0.25 mg mL^{-1}). We find it likely that in reality the value is somewhere in between these values.

Regarding the fitted values for $\Delta\mu_{\mathrm{ratio}}$ and to check for consistency, we show in the Supplementary Information that there is a relation between γ_{ratio} and $\Delta\mu_{\mathrm{ratio}}$. This relationship originates in the fact that both parameters depend on the solubility. The found relationship is consistent with our fitted values.

4. Conclusion

The large typical length scale of the polymer fiber networks seen in DT-PDPPTPT:[70]PCBM solar cells are too large for high solar cell performance, but can be used as a "model" system to study fiber formation in the semicrystalline polymers used in organic solar cells. The large fiber

width is relatively easy to analyze quantitatively, and we introduced three different quantification methods. We have investigated the effect of the most commonly used processing parameters on solar cell performance and correlate that to differences in fiber width. Surprisingly, we find that the fiber width is not significantly influenced by fullerene type, fullerene amount, drying rate, thermal annealing, and the amount of cosolvent. These experiments show that fiber width is *not* limited by ripening (growth after the depletion of free polymers). Only the molecular weight of the polymer and the type of cosolvent exert large effects on the fiber width. We attribute the changes in fiber width to the solubility of the polymer in the cosolvent and posit that these polymer fiber networks are formed in a process governed by nucleation-and-growth of free polymers. Our proposed model shows that solubility effects can indeed explain the observed trend in fiber width for devices processed from a ternary solvent blend. The results and conclusions drawn in this contribution show we can tune the length scale of the solar cell morphology by controlling the polymer solubility in the cosolvent. These findings will have to be verified for other polymer:fullerene combinations, preferably using quantitative methods. Understanding the origin of the morphological length scale will lead to improved optimization procedures for organic solar cells. Also, these results show why controlling solubility and molecular weight in the design of new polymers is crucial in the development of high-efficiency photoactive materials. The solubility of the polymer in the cosolvent is a convenient handle to control the typical size of fiber networks in polymer solar cells.

ASSOCIATED CONTENT

Supplementary information contains experimental details, information on the size quantification, detailed SEC data, more data series which did not make the main text due to space limitations, solubility data and the nucleation-and-growth model.

AUTHOR INFORMATION

Corresponding Author

r.a.j.janssen@tue.nl

Author Contributions

All authors have given approval to the final version of the manuscript.

Funding Sources

Dutch Polymer Institute (DPI), project #734.

Ministry of Education, Culture and Science (Gravity program 024.001.035).

Agency for Innovation by Science and Technology in Flanders (IWT).

Nederlandse Organisatie voor Wetenschappelijk Onderzoek (NWO).

ACKNOWLEDGMENT

This research forms part of the research programme of the Dutch Polymer Institute (DPI), project #734. The research is part of the Solliance OPV program and has received funding from the Ministry of Education, Culture and Science (Gravity program 024.001.035). G. Heintges acknowledges the Agency for Innovation by Science and Technology in Flanders (IWT) for funding. NWO is acknowledged for providing the beam time at the ESRF.

REFERENCES

(1) Krebs, F. C.; Espinosa, N.; Hösel, M.; Søndergaard, R. R.; Jørgensen, M. *Adv. Mater.* **2013**, *6*, 29.

(2) Yu, G.; Gao, J.; Hummelen, J. C.; Heeger, A. J. *Science* **1995**, *270*, 1789.

(3) Liu, F.; Gu, Y.; Shen, X.; Ferdous, S.; Wang, H.-W.; Russell, T. P. *Prog. Polym. Sci*. **2013**, *38*, 1990.

(4) Lee, J. K.; Ma, W. L.; Brabec, C. J.; Yuen, J.; Moon, J. S.; Kim, J. Y.; Lee, K.; Bazan, G. C.; Heeger, A. J. *J. Am. Chem. Soc.* **2008**, *130*, 3619.

(5) Peet, J.; Kim, J. Y.; Coates, N. E.; Ma, W. L.; Moses, D.; Heeger, A. J.; Bazan, G. C. *Nat. Mater.* **2007**, *6*, 497.

(6) Liao, H.-C.; Ho, C.-C.; Chang, C.-Y.; Jao, M.-H.; Darling, S. B.; Su, W.-F. *Mater. Today* **2013**, *16*, 326.

(7) Franeker, J. J.; Turbiez, M.; Li, W.; Wienk, M. M.; Janssen, R. A. J. *Nat. Commun.* **2015**, *6*, 6229.

(8) Liu, F.; Gu, Y.; Wang, C.; Zhao, W.; Chen, D.; Briseno, A. L.; Russell, T. P. *Adv. Mater.* **2012**, *24*, 3947.

(9) Jung, J. W.; Liu, F.; Russell, T. P.; Jo, W. H. *Energy Environ. Sci.* **2012**, *5*, 6857.

(10) Li, W.; Hendriks, K. H.; Furlan, A.; Roelofs, W. S. C.; Meskers, S. C. J.; Wienk, M. M.; Janssen, R. A. J. *Adv. Mater.* **2014**, *26*, 1565.

(11) Wang, D.; Liu, F.; Yagihashi, N.; Nakaya, M.; Ferdous, S.; Liang, X.; Muramatsu, A.; Nakajima, K.; Russell, T. P. *Nano Lett.* **2014**, *14*, 5727.

(12) Hedley, G. J.; Ward, A. J.; Alekseev, A.; Howells, C. T.; Martins, E. R.; Serrano, L. A.; Cooke, G.; Ruseckas, A.; Samuel, I. D. W. *Nat. Commun.* **2013**, *4*, 2867.

(13) Shaw, P. E.; Ruseckas, A.; Samuel, I. D. W. *Adv. Mater.* **2008**, *20*, 3516.

(14) Liu, Y.; Zhao, J.; Li, Z.; Mu, C.; Ma, W.; Hu, H.; Jiang, K.; Lin, H.; Ade, H.; Yan, He. *Nat. Commun.* **2014**, *5*, 5293.

(15) Kang, H.; Udding, M. A.; Lee, C.; Kim, K.-H.; Nguyen, T. L.; Lee, W.; Li, Y.; Wang, C.; Woo, H. Y.; Kim, B. J. *J. Am. Chem. Soc.* **2015**, *137*, 2359.

(16) Bartelt, J. A.; Douglas, J. D.; Mateker, W. R.; El Labban, A.; Tassone, C. J.; Toney, M. F. Fréchet, J. M. J.; Beaujuge, P. M.; McGehee, M. D. *Adv. Energy Mater.* **2014**, *4*, 1301733.

(17) Subbiah, J.; Purushothaman, B.; Chen, M.; Qin, T.; Gao, M.; Vak. D.; Scholes, F. H.; Chen, X.; Watkins, S. E.; Wilson, G. J.; Holmes, A. B.; Wong, W. W. H.; Jones, D. J. *Adv. Mater.* **2015**, *27*, 702.

(18) Liu, C.; Wang, K.; Hu, X.; Yang, Y.; Hsu, C.-H.; Zhang, W.; Xiao, S.; Gong, X.; Cao, Y. *ACS Appl. Mater. Interfaces* **2013**, *5*, 12163.

(19) Xiao, Z.; Sun, K.; Subbiah, J.; Qin, T.; Lu, S.; Purushothaman, B.; Jones, D. J.; Holmes, A. B.; Wong, W. W. H. *Polym. Chem.* **2015**, *6*, 2312.

(20) Shin, J.; Park, G. E.; Lee, D. H.; Um, H. A.; Lee, T. W.; Cho, M. J.; Choi, D. H. *ACS Appl. Mater. Interfaces* **2015**, *7*, 3280.

(21) Cao, X.; Li, M.; Liu, J.; Wang, H.; Zhou, K.; Han, Y. C *Org. Electron.* **2015**, *24*, 280.

(22) Kesava, S. V.; Fei, Z.; Rimshaw, A. D.; Wang, C.; Hexemer, A.; Asbury, J. B.; Heeney, M.; Gomez, E. D. *Adv. Energy Mater.* **2014**, *4*, 1400116.

(23) Canny, J. *IEEE Trans. Pattern Anal. Mach. Intell.* **1986**, *6*, 679.

(24) Duo, A. K.; Carter, D. R. *J. Orthop. Res.* **1991**, *9*, 918.

(25) Harrigan, T. P.; Mann, R. W. *J. Mater. Sci.* **1984**, *19*, 761.

(26) Wirix, M. J. M.; Bomans, P. H. H.; Hendrix, M. M. R. M.; Friedrich, H.; Sommerdijk, N. A. J. M.; de With, G. *J. Mater. Chem. A* **2015**, *3*, 5031.

(27) van Franeker, J. J.; Westhoff, D.; Turbiez, M.; Wienk, M. M.; Schmidt, V.; Janssen, R. A. J. *Adv. Funct. Mater.* **2015**, *25*, 855.

(28) Ballard, D. H.; Brown, C. M. *Computer Vision*; Prentice Hall: New Jersey, 1982 (p252).

(29) Lee, H. K. H.; Li, Z.; Constantinou, I.; So, F.; Tsang, S. W.; So, S. K. *Adv. Energy Mater.* **2014**, *4*, 1400768.

(30) Intemann, J. J.; Yao, K.; Yip, H.-L.; Xu, Y.-X.; Li, Y.-X.; Liang, P.-W.; Ding, F.-Z.; Li, X.; Jen, A. K.-Y. *Chem. Mater.* **2013**, *25*, 3188.

(31) Kouijzer, S.; Michels, J. J.; van den Berg, M.; Gevaerts, V. S.; Turbiez, M.; Wienk, M. M.; Janssen, R. A. J. *J. Am. Chem. Soc.* **2013**, *135*, 12057.

(32) Nilsson, S.; Bernasik, A.; Budkowski, A.; Moons, E. *Macromolecules* **2007**, *40*, 8291.

(33) Schaefer, C.; van der Schoot, P.; Michels, J. J. *Phys. Rev. E* **2015**, *91*, 022602.

(34) Li, G.; Shrotriya, V.; Yao, Y.; Yang, Y. *J. Appl. Phys.* **2005**, *98*, 043704.

(35) Verploegen, E.; Mondal, R.; Bettinger, C. J.; Sok, S.; Toney, M. F.; Bao, Z. *Adv. Funct. Mater.* **2010**, *20*, 3519.

(36) Li, W.; Hendriks, K. H.; Furlan, A.; Roelofs, W. S.; Wienk, M. M.; Janssen, R. A. J. *J. Am. Chem. Soc.* **2013**, *135*, 18942.

(37) Kim, J. H.; Lee, D. H.; Yang, D. S.; Heo, D. U.; Kim, K. H.; Shin, J.; Kim, H.-J.; Baek, K.-Y.; Lee, K.; Baik, H.; Cho, M. J.; Choi, D. H. *Adv. Mater.* **2013**, *25*, 4102.

(38) Groot, R. D. *J. Chem. Phys.* **2013**, *138*, 224904.

(39) Kashchiev, D. *Nucleation: Basic Theory with Applications*; Butterworth-Heinemann: Oxford, 2000.

(40) Mullin, J.W. *Crystallization*; Butterworth-Heinemann: Oxford, 2001.

(41) Schmidt, K.; Tassone, C. J.; Niskala, J. R.; Yiu, A. T.; Lee, O. P.; Weiss, T. M.; Wang, C.; Fréchet, J. M. J.; Beaujuge, P. M.; Toney, M. F. *Adv. Mater*. **2014**, *26*, 300.

(42) Israelachvili, J. N. *Intermolecular and surface forces (3th edition)*; Academic Press: Waltham (MA), 2011.

Graphic for TOC: